

# Structure of Hydrophobic Hydration of Benzene and Hexafluorobenzene from First Principles

Markus Allesch,<sup>†,‡</sup> Eric Schwegler,<sup>\*,‡</sup> and Giulia Galli<sup>‡,§</sup>

Department of Theoretical and Computational Physics, Graz University of Technology, Graz, Austria, Lawrence Livermore National Laboratory, P.O. Box 808, Livermore, California 94559, and University of California, Davis, Davis, California 95616

Received: August 22, 2006; In Final Form: October 29, 2006

We report on the aqueous hydration of benzene and hexafluorobenzene, as obtained by carrying out extensive (>100 ps) first principles molecular dynamics simulations. Our results show that benzene and hexafluorobenzene do not behave as ordinary hydrophobic solutes, but rather present two distinct regions, one equatorial and the other axial, that exhibit different solvation properties. While in both cases the equatorial regions behave as typical hydrophobic solutes, the solvation properties of the axial regions depend strongly on the nature of the  $\pi$ -water interaction. In particular,  $\pi$ -hydrogen and  $\pi$ -lone pair interactions are found to dominate in benzene and hexafluorobenzene, respectively, which leads to substantially different orientations of water near the two solutes. We present atomic and electronic structure results (in terms of Maximally Localized Wannier Functions) providing a microscopic description of benzene– and hexafluorobenzene–water interfaces, as well as a comparative study of the two solutes. Our results point at the importance of an accurate description of interfacial water to characterize hydration properties of apolar molecules, as these are strongly influenced by subtle charge rearrangements and dipole moment redistributions in interfacial regions.

## I. Introduction

Interactions between aromatic molecules and water play a key role in determining the properties of biophysical systems, including the structure of proteins, and molecular recognition processes. To examine the nature of these interactions, the aqueous solvation of benzene is often used as a simple model system. Although typically referred to as a hydrophobic solute,<sup>1,2</sup> benzene is actually capable of forming hydrogen bonds through its  $\pi$ -electrons. In particular, the slight electronegativity of carbon relative to hydrogen and the overall  $D_{6h}$  symmetry of benzene leads to a large negative quadrupole moment ( $\Theta = -33.3 \times 10^{-40} \text{ Cm}$ ),<sup>23</sup> which can act as a weak hydrogen bond acceptor with water.<sup>4–8</sup>

Experimentally, the interaction of benzene with water has been the subject of numerous studies with a variety of techniques, including NMR and resonant ion dip IR spectroscopy (see, e.g., refs 9–24). These investigations examined the solvation of benzene in liquid water, water in liquid benzene, as well as gas-phase benzene–water clusters. Although these studies have established various important properties such as solubilities and binding energies, they are not able to provide a detailed picture of the structural and electronic properties of the local hydration structure.

Theoretical studies based on empirical potentials and ab initio quantum chemical methods have focused on the water–benzene dimer<sup>2,25,26</sup> and small  $\text{C}_6\text{H}_6-(\text{H}_2\text{O})_n$  clusters.<sup>1,27,28</sup> For fully solvated species, all past investigations have been restricted to empirical potential models.<sup>29–38</sup>

In this paper, we investigate the structural and electronic properties of fully solvated benzene using first principles molecular dynamics (FPMD) for the first time. We have also compared benzene with hexafluorobenzene, which has similar structural properties, but a very different  $\pi$ -electron system, with an inverse quadrupole moment ( $\Theta = 31.7 \times 10^{-40} \text{ Cm}$ )<sup>23</sup> with respect to benzene.

As compared to benzene, very little is known about the interaction of hexafluorobenzene with water. Experimental studies on the dynamics of the solvation of water in hexafluorobenzene have been performed<sup>39</sup> but not vice versa. Theoretical studies have focused on the hexafluorobenzene–water dimer and found a preferred water orientation that is roughly opposite to the one found for the benzene–water dimer.<sup>40–43</sup> However, no experimental nor theoretical study on the solvation structure around fully solvated hexafluorobenzene has been reported to date. To the best of our knowledge, the simulations presented here are the first ab initio molecular dynamics studies of these two, fully solvated systems.

Simulating these aqueous solutions presents challenging size and time scale requirements because highly accurate simulations of the order of 100 ps are required to get statistically meaningful averages for structural properties. Therefore, we have used our previously developed rigid water approximation<sup>44</sup> to perform FPMD simulations of the different solutes for more than 100 ps, which constitute the most extensive simulations of its kind today. Our main goal is to understand the fundamental interactions between aromatic biomolecular building blocks and nature's most important solvent, at a molecular level. In addition, our comparison between benzene and hexafluorobenzene allows us to study the influence of charge distribution and quadrupole moments on structural and electronic properties of fully solvated aromatic systems.

<sup>†</sup> Graz University of Technology.

<sup>‡</sup> Lawrence Livermore National Laboratory.

<sup>§</sup> University of California, Davis.

## II. Method

We have performed FPMD simulations<sup>45,46</sup> of solvated benzene and hexafluorobenzene (HFB) under ambient pressure and temperature conditions. The simulations consist of 73 water molecules surrounding a benzene or HFB molecule in a periodically repeated cubic cell with a lateral dimension of 13.25 Å, which in the case of benzene is based on the experimentally measured molar volume of the solute.<sup>47,48</sup> The chosen size of the simulation box allows us to include the number of solvent molecules that are expected to be in the first and second solvation shells.<sup>30,31</sup>

All of our simulations were performed with the Car–Parrinello (CP) technique,<sup>49</sup> which uses a Lagrangian that couples together the system's electronic and ionic degrees of freedom.<sup>50</sup> The electronic structure was described within density functional theory (DFT)<sup>51,52</sup> with the PBE generalized gradient approximation (GGA).<sup>53</sup> The valence wave functions and charge density were expanded in a plane wave basis, which was truncated in reciprocal space at 85 and 340 Ry, respectively. Norm-conserving pseudopotentials of the Hamman type were used to describe valence-core interactions.<sup>54,55</sup>

Since the geometry of water molecules is not expected to change significantly in the vicinity of the solute<sup>25,40</sup> compared to its bulk values, we have utilized a rigid water model.<sup>44</sup> In addition to our previous study of pure rigid water we have also successfully applied this model to a solvated cation ( $\text{Ca}^{2+}$ ),<sup>56</sup> which gives us confidence in its suitability for the systems under consideration here. The use of a rigid water model permits the utilization of a larger fictitious mass in the CP dynamics, compared to flexible water and thus a larger MD time step.

The initial configurations for our ab initio studies were obtained from 100 ps classical MD simulations performed with the TINKER package.<sup>57</sup> To reach a temperature of approximately 300 K we have initially applied a weakly coupled velocity scaling thermostat for at least 3 ps in our ab initio simulations before removing the thermostat and collecting statistics within the NVE ensemble.

Three independent simulations were performed for benzene, and one continuous trajectory was calculated for HFB. The total ab initio simulation times for solvated benzene and HFB were 152.1 and 103.5 ps respectively with average temperatures of 303.3 and 299.1 K. Within the mentioned MD framework a 10 ps simulation of one of these systems takes about 26 h on 308 Itanium2 CPUs.

In addition to the 100 ps classical MD simulations that were used to obtain starting configurations, we have performed additional classical MD simulations to investigate the effects of simulation parameters such as size, time scales, and symmetry operations. The GROMACS 3.2.1 code<sup>58</sup> with the OPLSAA force field<sup>59</sup> and the TIP4P model for water<sup>60</sup> was used to obtain a series of uncorrelated 100 ps classical simulations to estimate the uncertainty in the distribution functions<sup>61</sup> of benzene solvated by 512 water molecules. This analysis will be presented in detail in a forthcoming publication.<sup>62</sup>

A central point in our analysis is the investigation of the electronic structure of water around the solutes. To this end, we have calculated maximally localized Wannier functions (MLWF) for several hundred configurations along our MD trajectories. The MLWF were computed “on the fly” following a joint approximate diagonalization scheme.<sup>63</sup> Besides our analysis of the positions and spreads of the Wannier function centers (WFC) we have also used the procedure of Silvestrelli et al.<sup>64</sup> to compute an approximate dipole moment of each of the water molecules in the simulation.

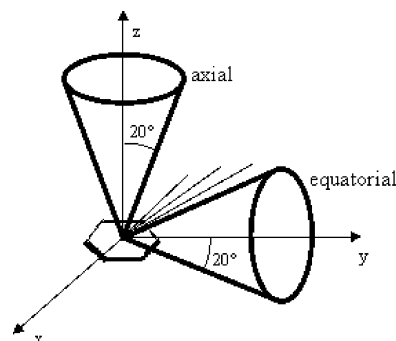


**Figure 1.** Definition of the axial and equatorial region around benzene and hexafluorobenzene. The equatorial region extends from the center of the solute in all directions throughout the  $xy$ -plane.

## III. Results and Discussion

To test the accuracy of our theoretical approach we have performed binding energy calculations of the benzene– $\text{H}_2\text{O}$  and HFB– $\text{H}_2\text{O}$  dimers within the aforementioned theoretical framework of DFT/PBE. For these calculations the optimized geometries were determined with the limited memory method of Broyden–Fletcher–Goldfarb–Shanno (LBFGS).<sup>65</sup> For benzene the distance from the center of the ring to the oxygen was found to have a very shallow minimum around 3.86 Å, which considering the constrained intramolecular geometry that is enforced in our calculations is in satisfactory agreement with previous quantum chemical studies (3.74 Å).<sup>42</sup> The preferred orientation of the optimized benzene– $\text{H}_2\text{O}$  dimer exhibits one hydrogen atom of water pointing at the  $\pi$ -cloud, in good agreement with both experimental and theoretical studies.

Using the same plane wave cutoff as in our simulations (85 Ry) we obtained binding energies of  $-1.91$  kcal/mol for benzene– $\text{H}_2\text{O}$  and  $-1.13$  kcal/mol for the HFB– $\text{H}_2\text{O}$  dimer. Increasing the energy cutoff to 120 Ry did not result in significantly different binding energies. For benzene– $\text{H}_2\text{O}$  our computed binding energy is consistent with quantum chemical results that have ranged from  $-1.50$  to  $-2.90$  kcal/mol depending on optimized geometry and level of theory.<sup>12,25,28,42,66</sup> For HFB, previous studies also exhibit a range of binding energies from  $-1.55$  to  $-2.69$  kcal/mol,<sup>40–43</sup> in satisfactory agreement with our calculations.

**A. Radial Distribution Functions.** A standard approach for describing the average structure of liquids and molecules in solution is to calculate the radial distribution function between atoms (RDF, or  $g(r)$ ). Earlier works have examined this quantity by using the carbon atoms of benzene as the reference point, which leads to a rather featureless  $g(r)$ . Here, we have used the benzene/HFB ring center as the reference point, which gives more structured RDFs and provides a clearer picture of the average structure of the liquid near the solute. The mirror plane symmetry of the solute molecule was exploited to improve statistics for all reported RDFs. We have also tested different bin sizes,  $\Delta r$ , from 0.01 to 0.09 Å to ensure independence of our reported RDFs from our discretization procedure. For all graphs shown in this section  $\Delta r = 0.03$  Å has proven to be a suitable choice. We have also divided the space around the solute into an equatorial and an axial region, since these areas exhibit distinctively different interactions (see Figure 1).

Figure 2 shows the average radial distribution of oxygen and hydrogen atoms in the equatorial and axial region using the solute center as a reference point. Results for solvated benzene and HFB are shown in the left and right column, respectively. The top panels compare the distribution around both solutes in the equatorial region ( $20^\circ$  on both sides of the plane defined by

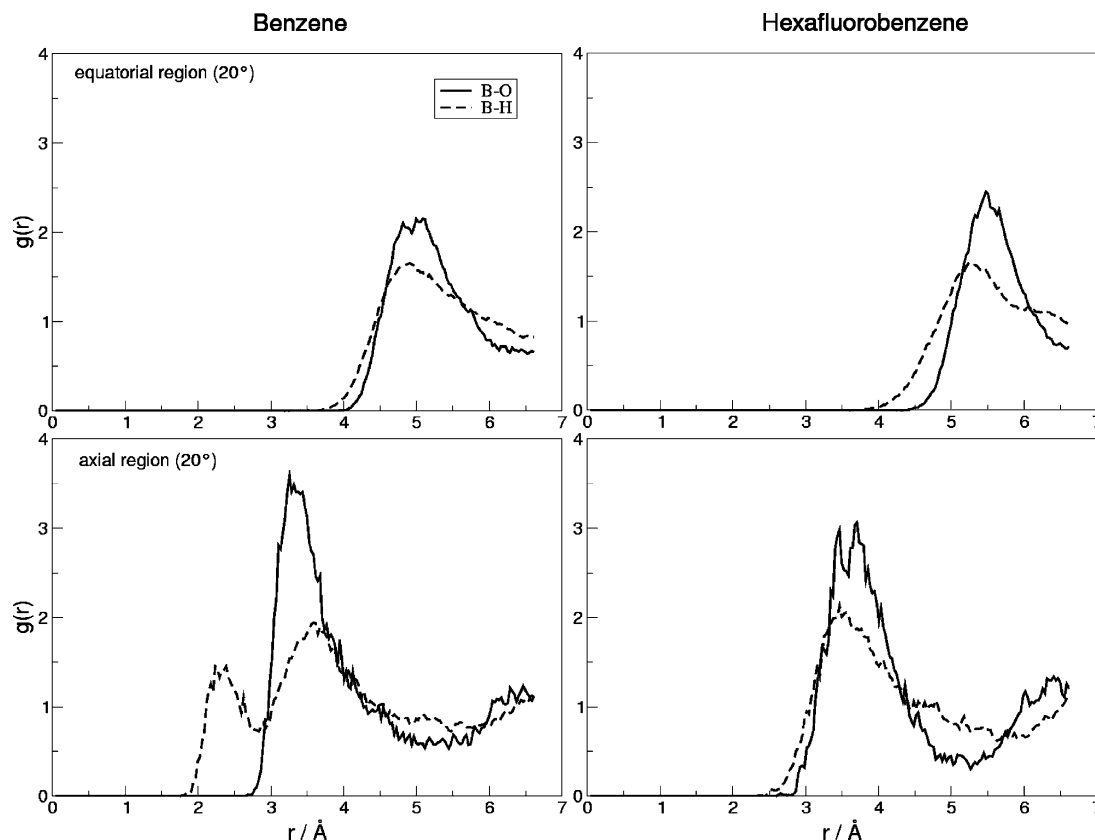


**Figure 2.** Solute center-oxygen (dashed lines) and solute center-hydrogen (solid lines) radial distribution functions in the equatorial and axial regions (see Figure 1). The left column shows RDFs for benzene (B), the right column the RDFs for hexafluorobenzene (HFB).

the solute molecule) whereas the bottom panels show the axial region (20° around the  $z$ -axis, defined perpendicular to the solute plane).  $g_{B-O}(r)$  in the equatorial region around benzene (top left) shows slightly more structure than the corresponding  $g_{B-H}(r)$  but both distributions are peaked around 4.9 Å with a similar onset located at 4.1 and 3.7 Å, respectively. In contrast, the distributions calculated from the axial region show a strong qualitative difference when compared to each other. The axial  $g_{B-H}(r)$  in Figure 2 displays a double peak with maxima at 2.3 and 3.6 Å, whereas the axial  $g_{B-O}(r)$  shows only one distinct maximum at 3.3 Å. The characteristic first  $g_{B-H}(r)$  peak, located at smaller distances (by about 1 Å) than the corresponding  $g_{B-O}(r)$  peak, suggests that there is a strong orientational preference for the water molecules near the axial region of benzene.

A similar analysis for water molecules surrounding HFB in the equatorial region (top right in Figure 2) shows  $g_{HFB-O}(r)$  shifted outward by approximately 0.6 Å, with a peak at 5.5 Å, and  $g_{HFB-H}(r)$  with a similar onset but a maximum shifted by about 0.4 Å when compared to the B-water system. While steric effects can explain a general outward shift of the  $g(r)$  in the equatorial region of HFB compared to solvated benzene, the difference between the  $g_{HFB-H}(r)$  and  $g_{HFB-O}(r)$  peaks (top right in Figure 2) has to be of a different origin, such as electrostatic effects stemming from the negative partial charge on the fluorine atoms.

The two  $g(r)$ s calculated from the axial region around HFB (bottom right in Figure 2) are qualitatively different from those obtained for the benzene-water system. Only one H-peak appears at 3.5 Å corresponding to the  $g_{HFB-O}(r)$  peak centered at 3.6 Å. The similar onset and shape of both distributions in Figure 2 suggest that any possible orientational effects on the faces of HFB must be of a different nature than in the case of

water on the faces of benzene. This will be further discussed in Section III.C. In the case of benzene, the axial  $g_{B-H}$ -double peak points at an orientation where the two hydrogen molecules of water are located at different distances from the solute center. Comparing peak positions in the axial regions to the optimized dimer geometries we notice that in the case of both benzene and HFB the condensed phase values for the solute center-oxygen distances are significantly smaller than in the gas phase. For both benzene and HFB, the overall structure of the water as described by the  $g_{O-O}(r)$ ,  $g_{O-H}(r)$ , and  $g_{H-H}(r)$  distribution functions (not shown) is very similar to those of pure water as described within the rigid approximation.<sup>44</sup>

**B. Spatial Distribution Functions.** To gain a better understanding of the three-dimensional local solvation structure, we have calculated spatial distribution functions (SDF)<sup>67</sup> of oxygen and hydrogen atoms around benzene and HFB. These SDFs depict the probability density distribution of the two solvent atoms in the first and second solvation shell around the two different solutes, similar to the concept of statistical state solvation sites.<sup>68</sup> Normalization of all SDF data has been performed with respect to the experimental bulk water density at ambient conditions. A common problem when trying to resolve solvation details around hydrophobic solutes is the long simulation time required to gather sufficient statistical data on spatial distributions.<sup>61</sup> We have overcome this difficulty by using the rigid water approximation, thus extending the timescales accessible by ab initio MD by a factor of 3,<sup>44</sup> and by exploiting all symmetry operations of the solute, so as to obtain sufficiently smooth SDF. To verify that no bias is introduced into our data by these symmetry operations, we have tested our SDF analysis on random distributions and large classical MD data sets.<sup>62</sup>

Figure 3 shows the distribution of oxygen (red) around benzene (top) and HFB (bottom) for two different isosurfaces.



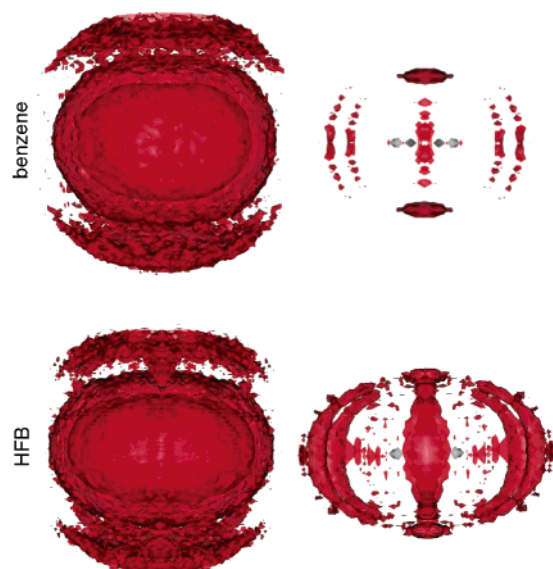


**Figure 3.** Spatial distribution function (shown in red) of oxygen around benzene (upper panel) and HFB (lower panel) illustrating the spheroidal shape (isosurface 1) on the left and the cage-like structure in the equatorial region of the first shell and the high concentration at the faces (isosurface 2.6) on the right. The spatial distribution of carbon is shown in gray. Due to the spheroidal shape of the second solvation shell compared to the cubic shape of the simulation box, the second shell is not fully represented within the MD cell.

The SDFs on the left illustrate the spheroidal shape of the first solvation shell and part of the second, whereas the right pictures show the distinct structures in the axial and equatorial region, which dominate within the first solvation shell. The cage-like oxygen density in the equatorial region around benzene (top right) is located in between the hydrogens of benzene and exhibits maxima in the equatorial plane. The axial region is characterized by a rather broad maximum of oxygen density around the  $C_6$ -symmetry axis of the molecule. Upon close inspection this axial oxygen density is found to have a torus-like shape.

The corresponding SDFs for hydrogen around benzene show a similar albeit less pronounced density in the equatorial region, and a clearly different distribution in the axial region. Figure 4 illustrates this difference between oxygen and hydrogen density distribution by showing both densities at an isosurface level of 1 for a  $90^\circ$  axial cone. Clearly visible are the two solvation shells with an additional region of hydrogen density much closer to the solute, which gives rise to the first hydrogen peak in the bottom left panel of Figure 2.

Another, more quantitative analysis of this data is shown in Figure 5. Plots of the  $yz$  and  $xy$  contour planes depict more pronounced oxygen SDFs in both regions, and a specific hydrogen density closer to the solute than the first solvation shell.

Analogous contour plots for oxygen and hydrogen densities around HFB (Figure 6) show several differences. In the equatorial region, oxygen shows higher densities and enhanced localization, i.e., a stronger cage-like structure. The hydrogen SDF contour plots show similar density values in the equatorial region but a somewhat broader spatial extension in the equatorial plane. Also, the equatorial extension of the solute cavity appears bigger, in part as a result of steric effects due to the fluorine atoms. In the axial region, a much more localized oxygen density and the total absence of the specific hydrogen density found for benzene are remarkable. In particular, the distribution of hydrogen atoms forms a broad disk on the faces. A direct

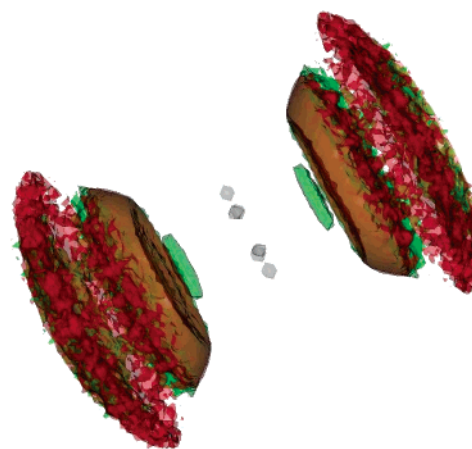


**Figure 4.** Combination of spatial distribution functions (isosurface 1) of oxygen and hydrogen around benzene in the axial region ( $45^\circ$  from  $z$ -axis). Oxygen is shown in red, hydrogen in green, and carbon in gray. In addition to the first and second solvation shell, a region of hydrogen density much closer to the benzene center is visible. The corresponding SDF for HFB looks almost identical except for the absence of this hydrogen density region.

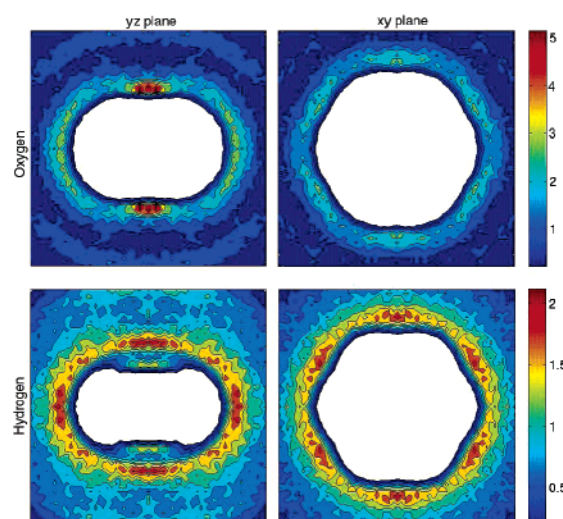


**Figure 5.** Contour planes ( $yz$  and  $xy$ ) through the oxygen- and hydrogen-spatial distribution functions (SDFs) of benzene

comparison is drawn in Figure 7 where a top view of the oxygen SDFs of solvated benzene and HFB is shown for the same isosurface.

**C. Angular Distribution Functions and Preferred Orientations.** The analysis of RDFs and SDFs has indicated that preferred orientations of water exist around benzene and possibly around HFB, particularly in the axial region. In this section, the orientations of water molecules are investigated depending on their position relative to the solute by calculating the tilt angles of individual  $H_2O$  molecules. As shown by Grossman et al. a first principles description is needed to accurately resolve angular preferences of solvent molecules around small hydrophobic molecules.<sup>69</sup> Again, the mirror symmetry of the solute has been exploited to improve statistics. A graphic definition of the polar angle and the tilt angle is given in Figure 8.

For benzene, the tilt angle distribution (Figure 9) shows a strong maximum axially at a tilt angle of  $\sim 46^\circ$  and a much weaker, rather broad distribution in the equatorial region around  $121^\circ$ . While the characteristic orientation in the axial region is concentrated in a very small region around the  $C_6$ -axis (i.e., around the maxima in the axial oxygen and hydrogen SDF, see

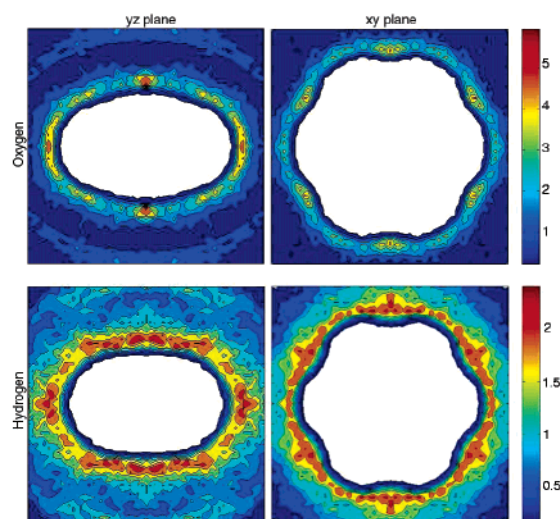


**Figure 6.** Contour planes (yz and xy) through the oxygen- and hydrogen-SDFs of HFB.

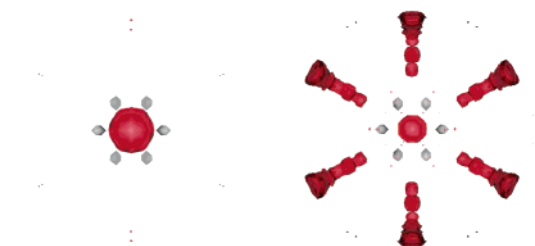


**Figure 7.** Top view of the spatial distribution function of oxygen around benzene (left) and HFB (right) for an isosurface of 3. Oxygen is shown in red and carbon atoms in gray; hydrogen and fluorine are not shown.

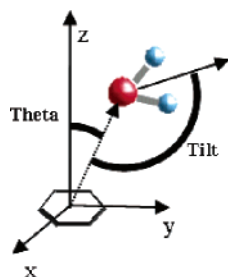


**Figure 8.** Definition of the water tilt angle used throughout this study (see text).

Figure 5) the equatorial orientation stretches much further and appears to be the preferred underlying orientation of water around these hydrophobic solutes, locally disrupted by a specific interaction of water on the faces. HFB yields a different picture in the axial region with a less pronounced maximum at  $\sim 123^\circ$  and again a very broad maximum in the equatorial region roughly around  $115^\circ$  (note that the colors in Figure 9 and 10 are scaled relative to their respective maxima). This preferred orientation of approximately  $120^\circ$ , which has also been found in a classical MD study of benzene and cyclohexane<sup>37</sup> and in a first principles study of solvated methane and silane,<sup>69</sup> appears to be a characteristic feature of water near small hydrophobic solutes. We also note that a smaller peak exists at  $\cos(\text{tilt}) = 1$  for both solutes representing small tilt angles. This has also been observed for other small hydrophobic molecules and was shown to arise from solvent molecules in the outer parts of the first solvation shell, whereas the dominant equatorial peak at  $\sim 120^\circ$  comes from molecules closest to the solute.<sup>69,70</sup>

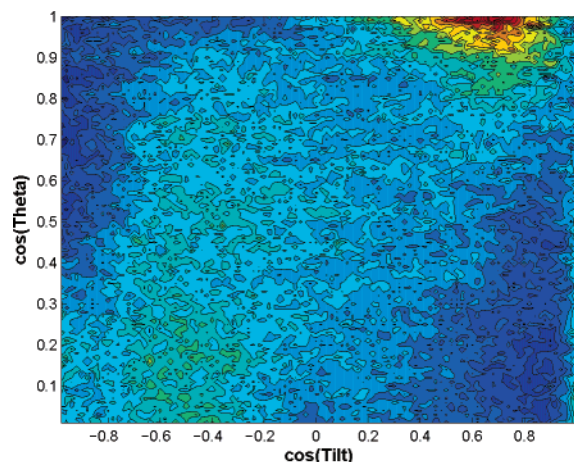


**Figure 9.** Cosine of the tilt angle of water molecules surrounding benzene up to a distance of 6.6 Å versus the polar angle  $\Theta$  measured from the  $C_6$  axis of the solute. The color map is scaled relative to the maximum.

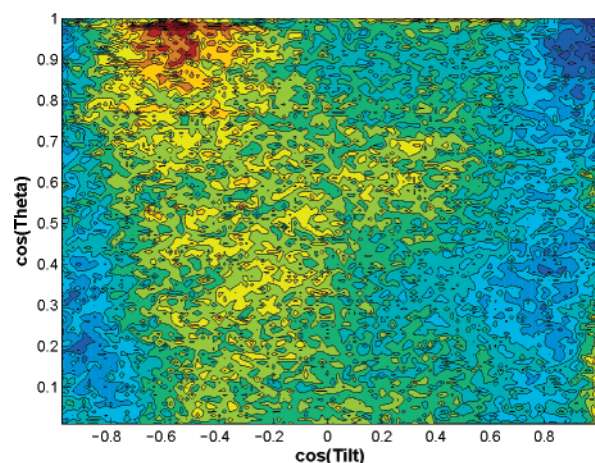


**Figure 10.** Cosine of the tilt angle of water molecules surrounding HFB up to a distance of 6.6 Å versus the polar angle  $\Theta$  measured from the  $C_6$  axis of the solute.

If one assumes that water tilt angles of  $\sim 120^\circ$  are characteristic of hydrophobic hydration of small apolar solutes, then Figures 9 and 10 nicely show why both molecules (benzene in particular) can be considered “atypical” hydrophobic solutes. While they show many characteristic properties, e.g., a large positive hydration heat capacity,<sup>71</sup> both solutes bind weakly to water molecules in the axial region leading to preferred orientations (i.e., the two dominant peaks in the axial region in Figures 9 and 10) which differ significantly from those commonly found around small hydrophobic solutes. While Figure 10 might suggest that HFB differs less from a normal hydrophobic solute than benzene, this is only true insofar as the axial interaction with  $H_2O$  is weaker. Still fully solvated HFB leads to different orientational preferences of water molecules in the axial region than expected around small apolar solutes, and this can be traced back to a distinct  $\pi$ -lone pair interaction.

Figure 11 shows a cartoon illustrating the two dominant orientations of water on the faces of benzene and HFB. Whereas the orientation of water on the faces of benzene is similar to the optimized gas-phase dimer (although the B—O distance is different), solvent molecules on the faces of HFB show a much smaller tilt angle than in the gas phase. Our geometry optimization as well as quantum chemical studies<sup>42</sup> have shown that the optimized HFB—water dimer displays a tilt angle of  $180^\circ$ , i.e.,



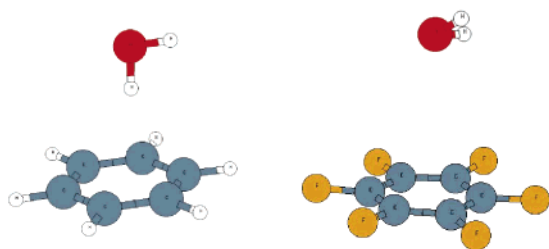


**Figure 11.** Characteristic orientation of water molecules bound to benzene and HFB.

oxygen pointing directly into the  $\pi$ -electron system. Despite this clear orientational preference in the axial region of both solutes, it is important to note that a high degree of freedom remains for the solvent molecules since a rotation around the  $C_6$ -axis of benzene will not change the preferred tilt angle. The broad hydrogen SDF in Figure 4 is a manifestation of this nonrigidity.

It is interesting to note that a recent computational study, which used classical potentials and Monte Carlo simulations to investigate orientational effects in the benzene–water interfacial region,<sup>72</sup> found that water molecules in the interface close to the apolar phase prefer to point one O–H bond toward the benzene phase, whereas water molecules on the aqueous side of the interface prefer to orient parallel to the interfacial plane. Benzene generally showed a preference to orient its plane parallel to the interface. The observed orientational preferences, although weaker at higher temperatures, and the radius of the first solvation shell were shown to be qualitatively independent of the thermodynamic conditions. These results agree qualitatively with the data presented here and highlight the importance of the environment on the relative orientation of benzene and water to each other.

**D. Electronic Properties.** One of the strengths of ab initio MD simulations comes from the inclusion of the electronic structure of the system at each step, including properties such as charge densities, charge transfer, and dipole moments. In the following section we investigate the differences between benzene and HFB in terms of their electronic structure and the peculiarities of the bonds established on the faces of benzene and HFB.

**1. MLWF Analysis.** After investigating details of the solvent structure and orientation, we analyzed the changes in electronic structure of the solutes and the solvent during our MD simulations to better understand the nature of their interactions. Maximally localized Wannier functions (MLWF)<sup>63,73</sup> offer an intuitive view of chemical bonds in condensed phases and an efficient way to explore the changes in electronic structure along MD trajectories.<sup>64</sup> Within the commonly used pseudopotential approximation there are four doubly occupied MLWF for each water molecule, 15 for benzene (6 localized on the C–H bonds and 9 for the  $\pi$ -electron system) and 33 for HFB (18 localized on F atoms, 6 localized on the C–F bonds, and 9 for the  $\pi$ -electron system).

First, we compare the  $\pi$ -electrons of benzene and HFB in terms of their spreads and their center's distance (WFC) from the molecule's plane. In the case of a delocalized  $\pi$ -electron system, the MLWFs resemble a series of single and double bonds, analogous to the classic Kekule representation. Figure 12 shows that the  $\pi$ -electrons of HFB exhibit a stronger localization in terms of both their MLWF spreads and WFC position; this can be understood in terms of the strong electronegativity of fluorine atoms. The effects of fluorination on the interaction of benzene dimer compounds have also been

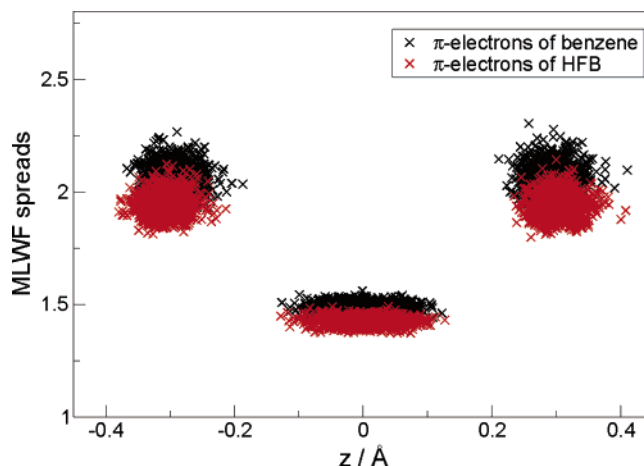


**Figure 12.** Spreads of the MLWFs belonging to the  $\sigma$ - and the  $\pi$ -electrons and the distance (denoted as  $z$ ) of their Wannier function centers from the plane defined by the faces of the solutes (fitted through the 6 C-atoms).

studied recently.<sup>74</sup> As expected, the substitution of fluorine onto the benzene molecule diminishes the partial negative character of the  $\pi$ -cloud above the ring and ultimately leads to a quadrupole moment that is similar in strength but opposite in sign. In Figure 11 we have identified the predominant orientation of water molecules that interact with the faces of benzene. We now analyze the corresponding changes that occur in the electronic structure of these interfacial  $H_2O$  molecules. To shed light on the nature of this specific interaction which “binds” one  $H_2O$  to the  $\pi$ -electron system of benzene and, to a lesser extent, to that of HFB we have compared the Wannier function centers (WFC) of binding  $H_2O$  molecules to those of bulk water molecules.

Figure 13 shows the oxygen–Wannier function center RDF, denoted as  $g_{OW}(r)$ , of the interacting  $H_2O$  molecule (dashed line) on the faces of benzene (left) and HFB (right) as well as the  $g_{OW}(r)$  of bulk water (solid line) for comparison. We have used 434/378 snapshots evenly spaced over the simulations of benzene/HFB, respectively, to compute these distributions. The reference curves of bulk water display two main peaks. The stronger peak at  $r \approx 0.33$  Å corresponds to the two oxygen lone pairs on each of the water molecules, whereas the smaller one centered at  $r \approx 0.49$  Å comes from the O–H covalent bonds. The gas-phase values are denoted as dotted lines. Comparing the reference distribution with  $g_{OW}(r)$  of the binding  $H_2O$  molecules on the faces of benzene (left graph in Figure 13) a strong shift of one binding O–H orbital centers toward the gas-phase value can be observed. In terms of conventional H-bonds Figure 13 suggests that the  $H_2O$  molecule donates a weak H-bond to the  $\pi$ -electron system of benzene.

For HFB (right graph in Figure 13) the binding water molecules also yield a different  $g_{OW}(r)$  than the reference bulk data, but in this case one of the lone pairs is affected, with its WFC shifted considerably closer to oxygen, essentially assuming its gas-phase value. This corresponds to the picture of a broken H-bond acceptor.

We have also compared the dipole moments of the “binding” water molecules on the faces of benzene to those of all other water molecules in the axial region. The dipole moments are calculated in an approximative manner from static configurations by assigning the total charge of the MLWF to a point charge at its center.<sup>64</sup> Figure 14 shows the dipole moment distribution of “binding”  $H_2O$  molecules compared to that of other axial first shell water molecules around benzene. Most notably the

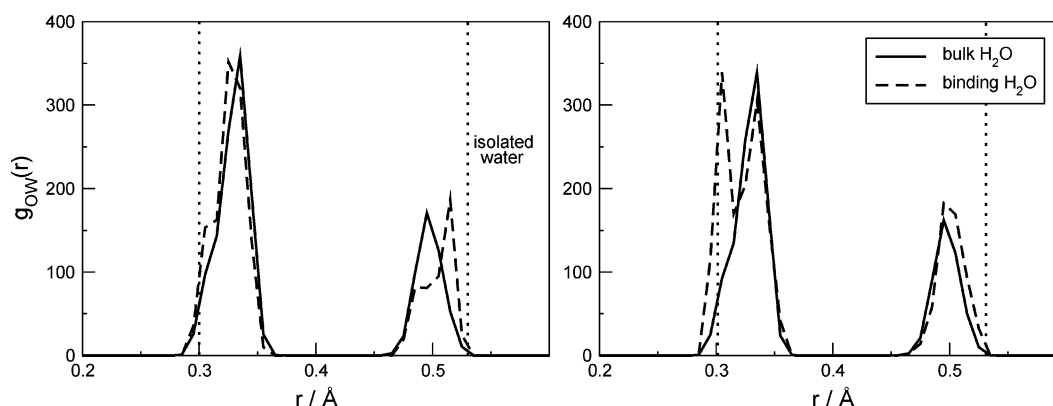


**Figure 13.** Oxygen-WFC radial distribution function for water molecules binding to the  $\pi$ -electron system of benzene (left) and HFB (right) compared to  $\text{H}_2\text{O}$  molecules in the bulk. Dotted lines represent the O-W distance for an isolated water molecule.

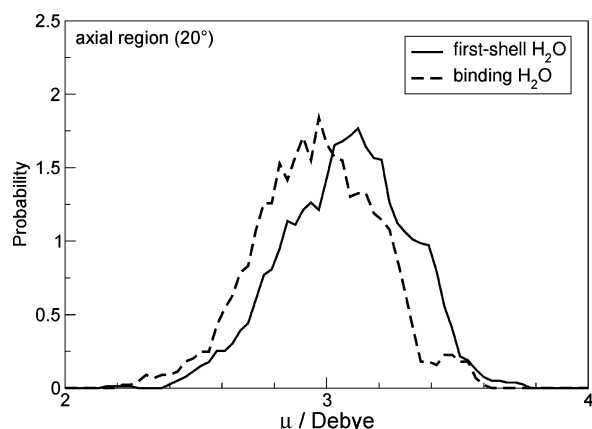


**Figure 14.** Calculated dipole moments of water in the axial region around benzene for two different radius intervals capturing the binding water molecules and the bulk water in the axial direction.

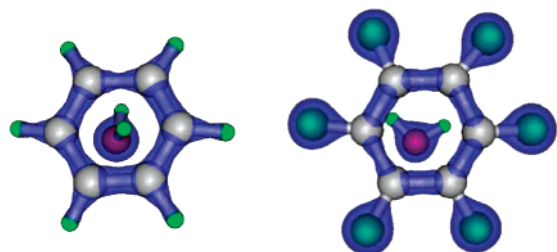


**Figure 15.** Total charge density plots for the unoptimized benzene-water and HFB-water dimer. Close inspection reveals the more localized charge distribution in the  $\pi$ -electron system of HFB, which is a result of the electron-withdrawing fluorine atoms.

$\pi$ -hydrogen interaction leads to a decrease in dipole moments by about 0.15 D, from 3.10 to 2.95 D. This behavior brings into question the suitability of classical nonpolarizable water models for MD simulations of solvated benzene.<sup>62</sup>

**2. Total Charge Density.** Another qualitative view on the changes in electronic structure caused by fluorination and upon binding to solvent molecules can be obtained by comparing the total charge densities of benzene-water and HFB-water dimers. These unoptimized dimers were cut out during the simulation from the full simulation cell and exhibit characteristic binding orientations (which were also shown in Figure 11). Figure 15 shows the slightly more localized charge density in the  $\pi$ -electron region of HFB caused by the substitution of fluorine (similar to Figure 12). It is important to note that in our electronic structure calculations utilizing pseudopotentials one electron for hydrogen is treated explicitly but four for each fluorine atom.

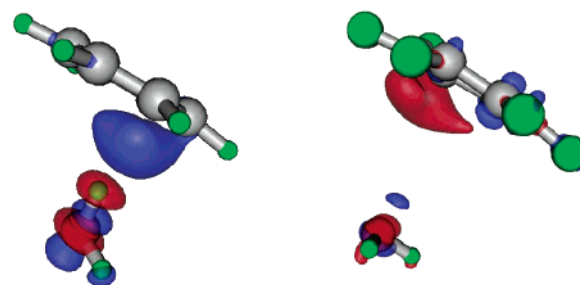


**Figure 16.** A qualitative comparison of charge density differences for the unoptimized benzene-water (left) and HFB-water dimer (right). Red indicates areas where the combined system contains less charge, blue where the charge density of the combined system is higher.

As noted earlier, fluorine substitution withdraws charge from the  $\pi$ -electron system leading to a more localized charge distribution in the  $\pi$ -plane and increases the partial charge on the fluorine atoms of HFB compared to the hydrogen atoms on benzene.<sup>74,75</sup>

Despite its usefulness for gaining a better understanding of the overall electronic structure of the dimers the total charge density does not clearly illustrate the subtle changes in electronic structure that occur upon formation of the respective dimers. Charge density difference plots of the benzene-water and HFB-water dimers point out regions with increased or decreased charge density compared to isolated solute and solvent molecules. We have also calculated charge density difference plots of the whole simulation cell; however, for clarity the results for the dimer are shown since it better allows one to inspect the important changes visually.

Figure 16 illustrates the transfer of charge from the  $\pi$ -system toward the hydrogen atom of  $\text{H}_2\text{O}$ , which points at the face of benzene and a loss of charge at the H atom accordingly. An opposite but smaller effect is found in the case of HFB where the  $\pi$ -system facing the water molecule shows charge depletion and the closest lone pair extends further, showing additional charge density closer to the  $\pi$ -system. A type of  $\pi$ -lone pair interaction in the case of solvated HFB can be inferred from this analysis. The same type of interaction but in a qualitatively different orientation has been observed for the gas-phase HFB-water dimer where both lone pairs symmetrically point toward the  $\pi$ -system.

Note that the charge density of an isolated (gas phase) water molecule is subtracted from the dimer and not the charge density of a bulk water molecule. Therefore, the charge density difference around water pointed out in Figure 16 refers to a gas-phase  $\text{H}_2\text{O}$  as a reference and not a bulk molecule (like previous comparisons in this section). The picture obtained from

charge density difference plots here is consistent with Figure 13, which compares only the WFC of binding and bulk water molecules. But while the lone pair distribution of water around HFB in Figure 13 suggests a broken H-bond, the analysis here shows that there is a notable transfer of charge toward the  $\pi$ -system although small compared to the case of benzene.

#### IV. Conclusion

In summary, we have reported the results of extensive ab initio simulations aimed at a microscopic description of the hydration structure of benzene and HFB. Our study represents the first investigation of these solutes in liquid water, obtained from first principles. Benzene and HFB are prototypical examples of solvated aromatic molecules that exhibit  $\pi$ -hydrogen and  $\pi$ -lone pair interactions, respectively. We have shown that both benzene and HFB are composed of two distinct regions: one equatorial and the other axial. The former behaves like an ordinary hydrophobic solute in the two aromatic molecules, although the cage-like structure shown in spatial distribution functions and characteristic of hydrophobic solutes is more pronounced in HFB than in benzene. The solvation of the axial region depends on how the  $\pi$ -electrons of the solute interact with interfacial water molecules. The axial region of benzene acts like an acceptor and forms a weak hydrogen bond with water (as shown, e.g., by our MLWF analysis), while HFB acts as a much weaker donor interacting with an oxygen lone pair. This specific behavior leads to different orientations of water on the faces of these solutes. The preferential tilt angle of water in the equatorial regions is about 120° for both benzene and HFB, while in the axial regions there is a strong preference for ~46° in benzene and ~123° in HFB. It is interesting to note that while the preferred orientation of water on the face of benzene is very similar in the gas-phase dimer and in liquid water, in the case of HFB the orientations found in the gas phase and in the liquid differ substantially. A similar difference in tilt angle distributions was found in recent cation solvation studies of  $\text{Mg}^{2+}$  and  $\text{Ca}^{2+}$ .<sup>56,76</sup>

The electronic structure of interfacial water molecules differs from that of bulk water, as a result of the interaction with the aromatic solute. In particular, we have found a decrease of the dipole moment by approximately 0.1 D in interfacial water molecules. These results indicate that the solvation of aromatic species is determined by subtle but important charge transfer and dipole redistribution effects, and cast some doubts on the validity of nonpolarizable models for the study of these systems. Our findings also indicate that electronic structure information, as contained in ab initio MD simulations, is an important component in a microscopic description of aromatic hydration.

**Acknowledgment.** The authors would like to thank G. Cicero for many useful discussions. M.A. was supported by a DOC fellowship of the Austrian Academy of Sciences. This work was performed under the auspices of the U.S. Department of Energy at the University of California/Lawrence Livermore National Laboratory under contract No. W-7405-Eng-48.

#### References and Notes

- (1) Sorenson, J. M.; Gregory, J. M.; Clary, D. C. *J. Chem. Phys.* **1997**, *106*, 849.
- (2) Cheng, B. M.; Grover, J. R.; Walters, E. A. *Chem. Phys. Lett.* **1995**, *232*, 364.
- (3) Vrbancich J.; Ritchie, G. L. D. *J. Chem. Soc., Faraday Trans. 2* **1980**, *76*, 648.
- (4) Nagy, P. I.; Ulmer, C. W., II; Smith, D. A. *J. Chem. Phys.* **1995**, *102*, 6812.
- (5) Alkorta, I.; Rozas, I.; Elguero, J. *Chem. Soc. Rev.* **1998**, *27*, 163.
- (6) Desiraju, G.; Steiner, T. *The weak Hydrogen Bond*; Oxford University Press: Oxford, UK, 2001.
- (7) Hübner, O.; Glöck, A.; Fichtner, M.; Kloppe, W. *J. Phys. Chem. A* **2004**, *108*, 3019.
- (8) Kim, K. S.; Tarakeshwar, P.; Lee, J. Y. *Chem. Rev.* **2000**, *100*, 4145.
- (9) Thompson, W. H.; Snyder, J. R. *J. Chem. Eng. Data* **1964**, *9*, 516.
- (10) Connolly, J. F. *J. Chem. Eng. Data* **1966**, *11*, 13.
- (11) Alwani, Z.; Schneider, G. *Ber. Bunsen-Ges. Phys. Chem.* **1967**, *71*, 633.
- (12) Suzuki, S.; et al. *Science* **1992**, *257*, 942.
- (13) Nakahara, M.; Wakai, C.; Yoshimoto, Y.; Matubayashi, N. *J. Phys. Chem.* **1996**, *100*, 1345.
- (14) Zwier, T. S. *Annu. Rev. Phys. Chem.* **1996**, *47*, 205.
- (15) Furutaka, S.; Ikawa, S. *J. Chem. Phys.* **1998**, *108*, 5159.
- (16) Furutaka, S.; Ikawa, S. *J. Chem. Phys.* **1998**, *108*, 1347.
- (17) Furutaka, S.; Ikawa, S. *J. Chem. Phys.* **2000**, *113*, 1942.
- (18) Furutaka, S.; Ikawa, S. *J. Chem. Phys.* **2002**, *117*, 751.
- (19) Bruant, R.; Conklin, M. *J. Phys. Chem. B* **2000**, *104*, 11146.
- (20) Jin, Y.; Ikawa, S. *J. Chem. Phys.* **2005**, *122*, 024509.
- (21) Gruenloh, C. J.; et al. *Science* **1997**, *276*, 1678.
- (22) Gruenloh, C. J.; et al. *J. Chem. Phys.* **2000**, *113*, 2290.
- (23) Gruenloh, C. J.; et al. *J. Chem. Phys.* **1998**, *109*, 6601.
- (24) Lee, J. Y.; et al. *J. Chem. Phys.* **2000**, *113*, 6160.
- (25) Feller, D. *J. Phys. Chem. A* **1999**, *103*, 7558.
- (26) Augspurger, J. C.; Dykstra, E.; Zwier, T. S. *J. Phys. Chem.* **1992**, *96*, 7252.
- (27) Fredericks, S. Y.; Jordan, K. D.; Zwier, T. S. *J. Phys. Chem.* **1996**, *100*, 7810.
- (28) Upadhyay, D. M.; Mishra, P. C. *J. Mol. Structure (THEOCHEM)* **2002**, *584*, 113.
- (29) Ravishanker, G.; Mehrotra, P. K.; Mezei, M.; Beveridge, D. L. *J. Am. Chem. Soc.* **1984**, *106*, 4102.
- (30) Linse, P.; Karlström, G.; Jansson, B. *J. Am. Chem. Soc.* **1984**, *106*, 4096.
- (31) Linse, P. *J. Am. Chem. Soc.* **1990**, *112*, 1744.
- (32) Jorgensen, W. L.; Severance, D. L. *J. Am. Chem. Soc.* **1990**, *112*, 4768.
- (33) Urahata, S.; Coutinho, K.; Canuto, S. *Chem. Phys. Lett.* **1997**, *274*, 269.
- (34) Urahata, S.; Canuto, S. *Chem. Phys. Lett.* **1999**, *31*, 3, 235.
- (35) Laaksonen, A.; Stills, P.; Wasylishen, R. E. *J. Chem. Phys.* **1998**, *108*, 455.
- (36) Raschke, T. M.; Levitt, M. *J. Phys. Chem. B* **2004**, *108*, 13492.
- (37) Raschke, T. M.; Levitt, M. *PNAS* **2005**, *102*, 6777.
- (38) Schravendijk, P.; van der Vegt, N. F. A. *J. Chem. Theory Comput.* **2005**, *1*, 643.
- (39) Besnard, M.; Danten, Y.; Tassaing, T. *J. Chem. Phys.* **2000**, *113*, 3741.
- (40) Danten, Y.; Tassaing, T.; Besnard, M. *J. Phys. Chem. A* **1999**, *103*, 3530.
- (41) Alkorta, I.; Rozas, I.; Jimeno, M. L.; Elguero, J. *Struct. Chem.* **2001**, *12*, 459.
- (42) Raimondi, M.; et al., *J. Phys. Chem. A* **2003**, *107*, 772.
- (43) Gallivan, J. P.; Dougherty, D. A. *Org. Lett.* **1999**, *1*, 103.
- (44) Allesch, M.; Schwegler, E.; Gygi, F.; Galli, G. *J. Chem. Phys.* **2004**, *120*, 5192.
- (45) Gygi, F. *GP 1.24.0*, A general ab initio molecular dynamics program; Lawrence Livermore National Laboratory, 2003.
- (46) Gygi, F. *The Qbox code*; Lawrence Livermore National Laboratory, 2005.
- (47) Dutta-Choudhury, M. K.; Miljevic, N.; van Hook, W. A. *J. Phys. Chem.* **1982**, *86*, 1711.
- (48) Tucker, E. E.; Christian, S. D. *J. Chem. Phys.* **1979**, *83*, 426.
- (49) Car, R.; Parrinello, M. *Phys. Rev. Lett.* **1985**, *55*, 2471.
- (50) Galli, G.; Parrinello, M. In *Computer Simulation in Materials Science*; Meyer, M.; Pontikis, V., Eds.; Kluwer Academic Publishers: Dordrecht, The Netherlands, 1991; pp 283–304.
- (51) Hohenberg, P.; Kohn, W. *Phys. Rev. B* **1964**, *136*, 864.
- (52) Kohn, W.; Sham, L. *J. Phys. Rev. A* **1965**, *140*, 1133.
- (53) Perdew, J. P.; Burke, K.; Ernzerhof, M. *Phys. Rev. Lett.* **1998**, *80*, 891.
- (54) Hamann, D. R. *Phys. Rev. B* **1989**, *40*, 2980.
- (55) Kleinman, L.; Bylander, D. M. *Phys. Rev. Lett.* **1982**, *48*, 1425.
- (56) Lightstone, F. C.; et al. *ChemPhysChem* **2005**, *6*, 1745.
- (57) *TINKER - Software Tools for Molecular Design*, Version 3.9.
- (58) Lindahl, E.; Hess, B.; van der Spoel, D. *J. Mol. Model.* **2001**, *7*, 306.
- (59) Kaminski, G.; Duffy, E.; Matsui, T.; Jorgensen, W. *J. Phys. Chem.* **1994**, *98*, 13077.
- (60) Jorgensen, W. L.; Madura, J. D. *Mol. Phys.* **1985**, *56*, 1381.
- (61) Grossman, J. C.; et al. *J. Chem. Phys.* **2004**, *120*, 300.



- (62) Allesch, M.; Lightstone, F. C.; Schwegler, E.; Galli, G. In preparation, 2006.
- (63) Gygi, F.; Fattebert, J. L.; Schwegler, E. *Comput. Phys. Commun.* **2003**, 155, 1.
- (64) Silvestrelli, P. L.; Parrinello, M. *Phys. Rev. Lett.* **1999**, 82, 3308.
- (65) Liu, D. C.; Nocedal, J. *Math. Programming* **1989**, 45, 503.
- (66) Courty, A.; et al. *J. Phys. Chem. A* **1998**, 102, 6590.
- (67) Svishchev, I. M.; Zassetsky, A. Y.; Kusalik, P. G. *Chem. Phys.* **2000**, 258, 181.
- (68) Mehrotra, P. K.; Marchese, F. T.; Beveridge, D. L. *J. Am. Chem. Soc.* **1981**, 103, 672.
- (69) Grossman, J. C.; Schwegler, E.; Galli, G. *J. Phys. Chem. B* **2004**, 108, 15865.
- (70) Koh, C. A.; et al. *J. Chem. Phys.* **2000**, 113, 6390.
- (71) Hummer, G.; Garde, S.; Garcia, A.; Pratt, L. *Chem. Phys.* **2000**, 258, 349.
- (72) Kereszturi, A.; Jedlovsky, P. *J. Chem. Phys. B* **2005**, 109, 16782.
- (73) Marzari, N.; Vanderbilt, D. *Phys. Rev. B* **1997**, 56, 12847.
- (74) Riley, K.; Merz, K. M. *J. Phys. Chem. B* **2005**, 109, 17752.
- (75) Fowler, P. W.; Steiner, E. *J. Phys. Chem.* **1997**, 101, 1409.
- (76) Lightstone, F. C.; et al. *Chem. Phys. Lett.* **2001**, 343, 549.